UC Irvine
UC Irvine Previously Published Works

Title

Chloride Ligands on DNA-Stabilized Silver Nanoclusters

Permalink

https://escholarship.org/uc/item/9cj5s11x

Journal

Journal of the American Chemical Society, 145(19)

ISSN

0002-7863

Authors

Gonzàlez-Rosell, Anna
Malola, Sami
Guha, Rweetuparna
et al.

Publication Date

2023-05-17

DOI

10.1021/jacs.3c01366

Peer reviewed

Chloride Ligands on DNA-Stabilized Silver Nanoclusters

Anna Gonzàlez-Rosell, Sami Malola, Rweetuparna Guha, Nery R. Arevalos, María Francisca Matus, Meghen E. Goulet, Esa Haapaniemi, Benjamin B. Katz, Tom Vosch, Jiro Kondo, Hannu Häkkinen, and Stacy M. Copp*

ACCESS | Metrics & More | Article Recommendations | Supporting Information

ABSTRACT: DNA-stabilized silver nanoclusters (Ag$_N$-DNAs) are known to have one or two DNA oligomer ligands per nanocluster. Here, we present the first evidence that Ag$_N$-DNA species can possess additional chloride ligands that lead to increased stability in biologically relevant concentrations of chloride. Mass spectrometry of five chromatographically isolated near-infrared (NIR)-emissive Ag$_N$-DNA species with previously reported X-ray crystal structures determines their molecular formulas to be $(DNA)_2[Ag_{16}Cl_2]^{8+}$. Chloride ligands can be exchanged for bromides, which red-shift the optical spectra of these emitters. Density functional theory (DFT) calculations of the 6-electron nanocluster show that the two newly identified chloride ligands were previously assigned as low-occupancy silvers by X-ray crystallography. DFT also confirms the stability of chloride in the crystallographic structure, yields qualitative agreement between computed and measured UV−vis absorption spectra, and provides interpretation of the ^{35}Cl-nuclear magnetic resonance spectrum of $(DNA)_2[Ag_{16}Cl_2]^{8+}$. A reanalysis of the X-ray crystal structure confirms that the two previously assigned low-occupancy silvers are, in fact, chlorides, yielding $(DNA)_2[Ag_{16}Cl_2]^{8+}$. Using the unusual stability of $(DNA)_2[Ag_{16}Cl_2]^{8+}$ in biologically relevant saline solutions as a possible indicator of other chloride-containing Ag$_N$-DNAs, we identified an additional Ag$_N$-DNA with a chloride ligand by high-throughput screening. Inclusion of chlorides on Ag$_N$-DNAs presents a promising new route to expand the diversity of Ag$_N$-DNA structure−property relationships and to imbue these emitters with favorable stability for biophotonics applications.
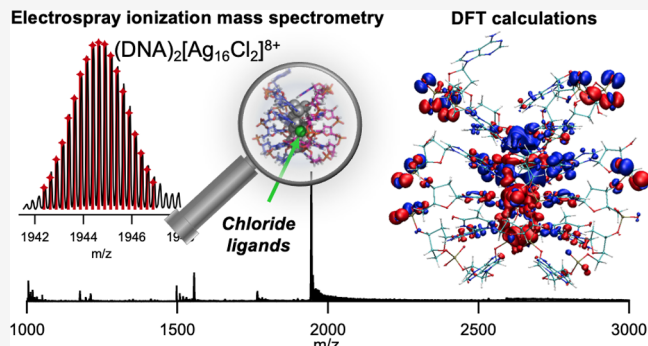
INTRODUCTION

DNA-stabilized silver nanoclusters (Ag$_N$-DNAs) are a diverse class of emitters that hold promise for bioimaging and biosensing.[1−6] Ag$_N$-DNAs have been reported with wide-ranging emission wavelengths from 400 to 1200 nm,[7,8] emission lifetimes from nanoseconds to microseconds,[9−12] and favorably high quantum yields and extinction coefficients.[13−15] The combinatorial nature of DNA ligand sequences is responsible for the diversity of Ag$_N$-DNA emitters, with nucleobase sequence selecting Ag$_N$ composition and photophysical properties.[16,17] These emitters can exhibit dark states that enable optically activated delayed fluorescence (OADF),[18,19] dielectric sensitivity,[14] and quantum beating.[20] Many Ag$_N$-DNAs have been reported to undergo analyte-induced transformations that enable chemical sensing schemes,[2] and a growing class of near-infrared (NIR)-emissive Ag$_N$-DNAs[8,21,22] hold promise for NIR bioimaging.[15,23−26]

While Ag$_N$-DNAs and other biomolecule-stabilized nanoclusters remain less understood than monolayer-protected nanoclusters,[27] studies of compositionally pure Ag$_N$-DNA samples have significantly advanced knowledge about these emitters in the last decade. Specific Ag$_N$-DNA species can be isolated from the multitude of other synthesis byproducts by

high-performance liquid chromatography (HPLC),[17] and the mass and charge of the nanocluster species can then be resolved by high-resolution electrospray ionization mass spectrometry (ESI-MS) in negative ion mode.[13,28] By this method, researchers have shown that emissive Ag$_N$-DNAs contain $N = 10−30$ Ag atoms and one or two copies of the stabilizing DNA oligomer.[13,21,29]

ESI-MS has also been used to determine the effective valence electron count of Ag$_N$-DNAs, which is necessary for accurate electronic structure calculations.[30] (Due to the valency of silver, this electron count has previously been referred to as the number of effective neutral silver atoms, N_0, in the Ag$_N$-DNA core.[13]) ESI-MS shows that like other ligand-protected nanoclusters, Ag$_N$-DNAs are partially oxidized, i.e., $N_0 < N$,[13,28] and that the excited-state behavior of Ag$_N$-DNA
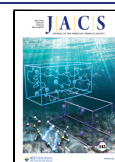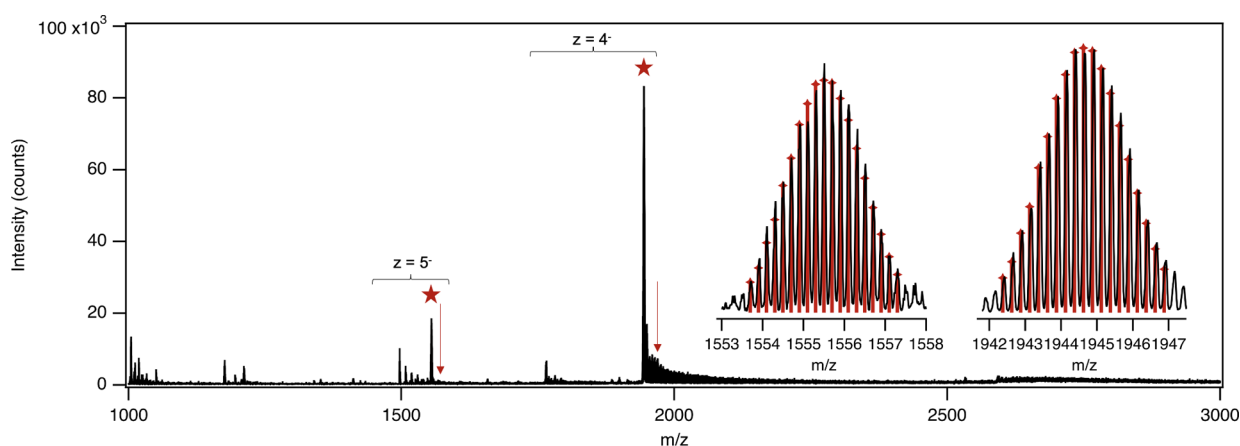
Figure 1. ESI mass spectrum of $(DNA)_2[Ag_{16}Cl_2]^{8+}$. Insets show calculated isotopic distributions (red lines) aligned with experimental peaks (black curve) at $z = 5^-$ and $z = 4^-$, as indicated by red stars. Red arrows show the predicted position for $(DNA)_2[Ag_{18}]^{q+}$.

emitters depends strongly on N_0. Ag_N-DNAs with nanosecond-lived fluorescence have N_0 values of 4, 6, and 10−12 that scale strongly with excitation and emission wavelengths, consistent with the rod-like geometry of these fluorescent Ag_N-DNAs.[13,14,29] A newly reported class of Ag_N-DNAs with a spherical superatomic magic number $N_0 = 8$ exhibits distinct UV−vis spectra and microsecond-lived luminescence rather than fluorescence.[12] Thus, it is clear that N_0 plays an important role in the Ag_N-DNA electronic structure.

The first X-ray crystal structures of Ag_N-DNAs were recently published,[7,31−34] providing the exciting possibility of theoretically solving the electronic structure of Ag_N-DNAs for the first time. However, complementary ESI-MS has not yet assigned N_0 to Ag_N-DNAs with solved crystal structures. Here, we seek to determine N_0 for the series of rod-like NIR-emissive Ag_{16}-DNAs reported by Cerretani et al.,[31−33] which can be purified by HPLC for detailed correlation of photophysical and structural properties of the emissive species.[31] Unexpectedly, we find that these emitters have composition $(DNA)_2[Ag_{16}Cl_2]^{8+}$, which is the first time that Ag_N-DNAs have been reported with additional chloride ligands. Ligand exchange of chlorides to bromides confirms the halide nature of these "extra" ligands. Density functional theory (DFT) calculations and reanalysis of the X-ray crystal structure show that these chloride ligands were the two atoms that were previously assigned as low-occupancy silvers.[31−33] DFT-calculated optical absorbance for the six-electron system agrees well with the experiment, and DFT calculations also explain the presence of two distinct resonances in the ^{35}Cl-nuclear magnetic resonance (NMR) spectrum of $(DNA)_2[Ag_{16}Cl_2]^{8+}$ and reveal solvent-accessible "channels" that may enable halide exchange. Using the unusual chemical stability of the chloride-containing $(DNA)_2[Ag_{16}Cl_2]^{8+}$ as an indicator of possible chloride ligands on other Ag_N-DNAs, we use high-throughput experimental screening to show that other Ag_N-DNAs can also possess chloride ligands. Our findings present a promising new way to achieve Ag_N-DNAs with suitable chemical stabilities for biomedical applications.

■ RESULTS AND DISCUSSION

Mass Spectral Analysis. The NIR-emissive Ag_N-DNA stabilized by the DNA oligomer 5′-CACCTAGCGA-3′ was synthesized and purified by HPLC, yielding a product with peak absorbance at 525 nm and peak emission at 735 nm

(Figures S1 and S2), as reported by Bogh et al.[23] Cerretani et al. previously used X-ray crystallography to show that this rod-shaped nanocluster is stabilized by two copies of the DNA template strand and identified the nanocluster as Ag_{16}, with two additional atoms assigned as silvers with low occupancies of ∼0.3.[31] Based on these past findings, the total mass of the nanocluster is expected to correspond to the masses of two DNA oligomers and either 16, 17, or 18 silvers.

We performed ESI-MS to determine the mass and electron count N_0 of this NIR-emissive species using previously established methods.[3,13] The experimentally measured mass spectrum for the purified species shows well-resolved individual peaks (Figure 1) that, unexpectedly, do not correspond to any integer numbers of DNA strands and silver atoms. The two dominant peaks at 1555 and 1945 m/z correspond to the 5^- and 4^- charge states, respectively, of a product that lies between the calculated isotopic distributions for $(DNA)_2Ag_{16}$ and $(DNA)_2Ag_{17}$ of various cluster charges (Figure S8). These peaks also do not correspond to higher mass adducts of Ag_N-DNA species with Na^+ or NH_4^+, which are commonly observed in ESI-MS for Ag_N-DNAs and other DNA complexes.[12,35] Instead, the experimental mass spectrum matches the predicted isotopic distribution for a product composed of 2 DNA strands, 16 Ag atoms, and 2 Cl atoms, with a total nanocluster charge of $q = 8$: $(DNA)_2[Ag_{16}Cl_2]^{8+}$. This corresponds to a nanocluster with $N_0 = 6$ effective valence electrons.[30] Electron counts of $N_0 = 6$ have been reported for rod-like red-emissive Ag_N-DNAs with peak absorption wavelengths similar to the NIR-emissive species studied here.[29,36] Adducts of $(DNA)_2[Ag_{16}Cl_2]^{8+}$ with Na^+ are also clearly resolved in the mass spectrum (Figure S11). Smaller mass products are formed by fragmentation during ESI, as is commonly observed for Ag_N-DNAs[12,17,21,29] and other non-covalent DNA complexes,[35] and these fragments are annotated in Figure S9.

It is plausible that the atoms that were previously assigned as silvers with low ∼0.3 occupancies in the reported crystal structure[31] are, instead, chloride ligands because Cl has 0.36 of the electron content of Ag. Chloride ligands have been found to be critical for formation of other ligand-protected silver nanoclusters[37,38] and to increase the sizes and structural diversity of nanoclusters.[39] Similarly sized elements do not explain the mass spectrum in Figure 1. Calculated isotopic distributions with K^+ and Ca^{2+} instead of Cl^- match the

experimental mass spectrum for nanocluster charges of $q = 15$ and $q = 17$, respectively, (Figure S12), but these compositions and charges correspond in both cases to an odd effective valence electron count of $N_0 = 3$. We find that the electron paramagnetic resonance (EPR) of the NIR-emissive species is silent (Figure S13), which is inconsistent with an odd valence electron count and consistent with the composition of the nanocluster as $(DNA)_2[Ag_{16}Cl_2]^{8+}$ and $N_0 = 6$.

Mass Spectral Analysis of Variant Nanoclusters. To further verify the presence of chloride ligands on the NIR-emissive species, we sized four variants of this emitter that X-ray crystallography showed to all possess the same core nanocluster structure of Ag_{16} with two additional low-occupancy silvers. Cerretani et al. reported that the nanocluster core structure is preserved when the thymine at position 5 on the original 10-base DNA ligand sequence is mutated to adenine, cytosine, or guanine (termed T5A, T5C, and T5G)[33] or when the terminal adenine at position 10 is removed (termed A10).[32] All four variant Ag_{16}-DNAs were prepared and purified in the same manner as the original $(DNA)_2[Ag_{16}Cl_2]^{8+}$ (Figures S3−S7). Figure 2 and Table S3 show that all variants' mass spectra are well-fitted to calculated distributions for $(DNA)_2[Ag_{16}Cl_2]^{8+}$.

Intentional Chloride Addition. Chloride ligands can be intentionally introduced using chlorine-containing solvents,[40] but researchers have also reported nanoclusters with unexpected chloride ligands, which are often surmised to form due to trace impurities[41,42] or adventitious sources.[43] In the case of Ag_N-DNAs, chloride-containing reagents are avoided during synthesis and purification to avoid precipitation of AgCl. While the exact source of the chloride ligands in the $(DNA)_2[Ag_{16}Cl_2]^{8+}$ species is unknown, Cl^- is a common impurity in plastics and glassware and can also be residually present from commercial solid-phase DNA oligomer synthesis. We observed large variability in the chemical synthesis yield of $(DNA)_2[Ag_{16}Cl_2]^{8+}$ when using different oligomer preparations from the commercial manufacturer (Figure S16), suggesting the presence of trace impurities in these synthetic DNA oligomers. Therefore, we tested the effect of controlled amounts of a chloride source on the chemical yield of $(DNA)_2[Ag_{16}Cl_2]^{8+}$ by first purifying the DNA oligomer by HPLC to remove residual salts and then adding controlled amounts of NH_4Cl to the nanocluster solution after reduction. This intentional addition of NH_4Cl resulted in a 2.7× increase in fluorescence emission (Figure S17).

Halide Ligand Exchange. Other halides have been used as ligands for metal nanoclusters.[44−46] For instance, a $N_0 = 6$ prolate-shaped Au_{10} nanocluster is stabilized by N-heterocyclic carbenes and two additional bromide ligands.[47] We confirm the halide nature of the "extra" ligands on $(DNA)_2[Ag_{16}Cl_2]^{8+}$ by exchanging the chlorides for bromides by adding NaBr to the purified $(DNA)_2[Ag_{16}Cl_2]^{8+}$ at 10×, 50×, 100×, and 500× excess of the concentration of Cl^- in the nanocluster solution. After addition of NaBr, the absorbance and emission peaks red-shift (Figure 3a,b), and the sample visually changes color from pink to purple (Figure S18). ESI-MS shows that Cl^- ions are partially substituted at lower concentrations of Br^-, with three different species in solution: $(DNA)_2[Ag_{16}Cl_2]^{8+}$, $(DNA)_2[Ag_{16}ClBr]^{8+}$, and $(DNA)_2[Ag_{16}Br_2]^{8+}$ (Figure S19). Higher concentrations of NaBr result in full substitution of chlorides for bromides (Figure 3c), and the fully substituted $(DNA)_2[Ag_{16}Br_2]^{8+}$ has absorbance and emission peaks of 541 and 765 nm, respectively. Further increasing $[Br^-]$ destabilizes
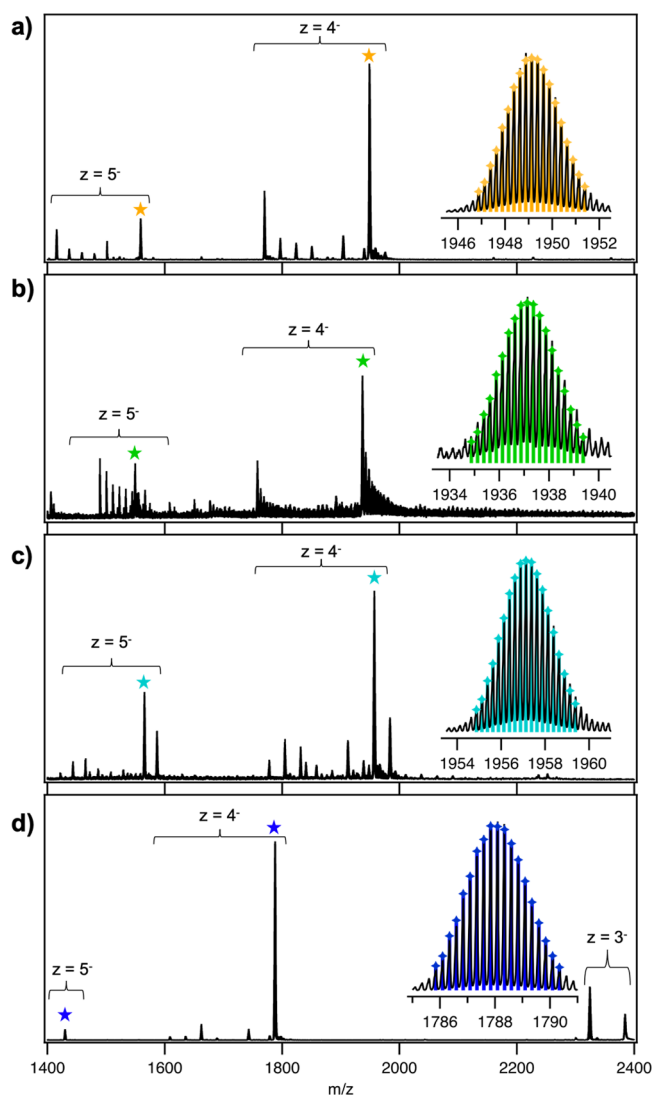

Figure 2. Mass spectra of (a) T5A-$(DNA)_2[Ag_{16}Cl_2]^{8+}$, (b) T5C-$(DNA)_2[Ag_{16}Cl_2]^{8+}$, (c) T5G-$(DNA)_2[Ag_{16}Cl_2]^{8+}$, and (d) A10-$(DNA)_2[Ag_{16}Cl_2]^{8+}$. Insets show isotopic distributions aligned with experimental peaks at $z = 4^-$ for each sample. Stars indicate peaks corresponding to insets with calculated isotopic distributions. Full mass spectra and fits can be found in Figures S14 and S15.

the nanocluster, and at 500× $[Br^-]$ (light pink in Figure 3a,b), $(DNA)_2[Ag_{16}Br_2]^{8+}$ is no longer present in significant quantity.

DFT Calculations. We performed a series of DFT calculations using the software GPAW[48] (see the Supporting Information for technical details) to investigate the stability of chloride in the observed crystallographic structure and its effect on the UV−vis absorption of the nanocluster species. For these calculations, we use the A10-$(DNA)_2[Ag_{16}Cl_2]^{8+}$ variant species (ref 32, PDB accession code 6M2P) because the crystal structure of the A10 variant was resolved to the highest resolution of all of the variants of the NIR emitter, and it has equivalent structure compared to the original NIR emissive species.[31] Figure 4 shows the isolated $[Ag_{16}X_2]^{q+}$ cluster core as taken from the crystallographic data, with the re-assigned atoms X shown in red. The total charge of the system is set to q. By fixing the 16 Ag (gray) atoms in the crystallographic sites and optimizing the positions of X atoms for X = Cl (green) and $q = 8$ (corresponding to the experimentally measured value of $N_0 = 6$, according to the superatom model[30]), we find
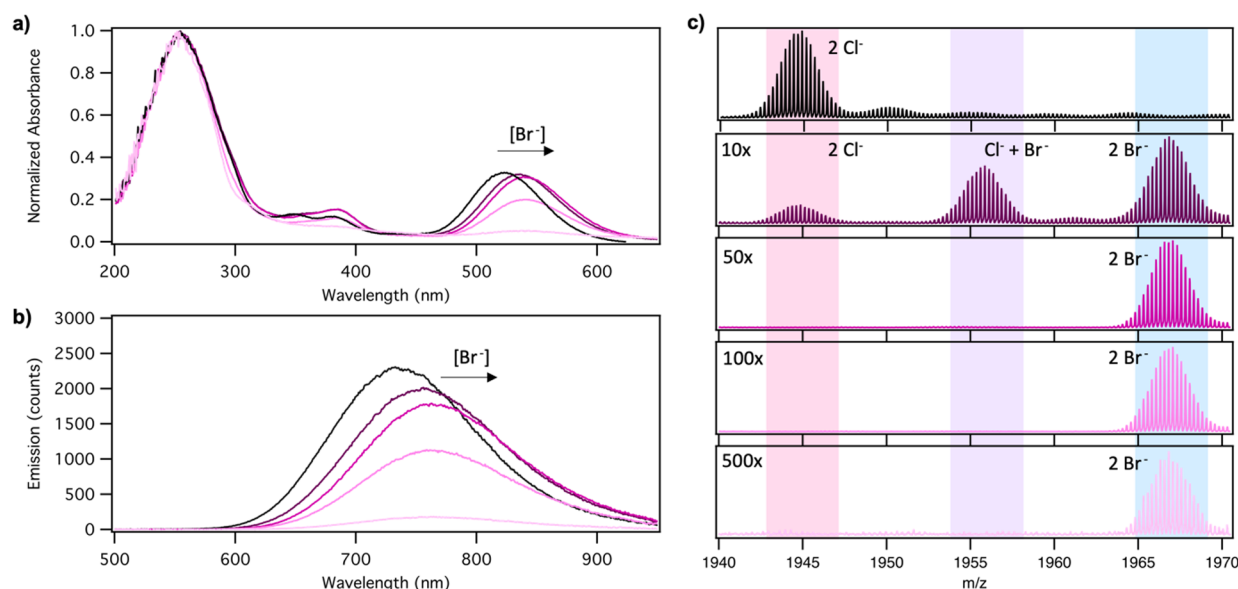
Figure 3. (a) Absorbance, (b) emission, and (c) ESI mass spectra confirm ligand exchange in the presence of excess Br^-, yielding $(DNA)_2[Ag_{16}Br_2]^{8+}$. All solutions were prepared using 12.5 μM $(DNA)_2[Ag_{16}Cl_2]^{8+}$, equivalent to 25 μM chloride concentration. The original $(DNA)_2[Ag_{16}Cl_2]^{8+}$ with no Br^- added is in black. Increasingly lighter shades of magenta indicate increased 10×, 50×, 100×, and 500× concentration of NaBr per chloride. (a, b) Arrows indicate red-shift in peak absorbance and peak emission with increasing $[Br^-]$. (c) Shading colors indicate mass spectral peaks for the different ligand compositions (calculated isotopic distributions and full mass spectra are shown in Figures S19 and S20).
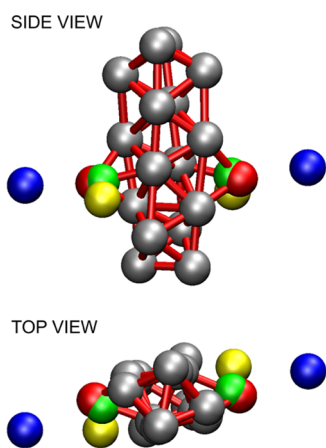

Figure 4. Isolated cluster model $[Ag_{16}X_2]^{q+}$ for testing the stability of the two atoms X in the observed crystal structure with DFT calculations. Gray spheres show the crystallographic sites of the 16 Ag atoms. Red spheres show the crystallographic positions of the X atoms. Green spheres show the DFT-optimized positions for X = Cl with q = 8 (corresponding to $N_0 = 6$ delocalized electrons in the nanocluster). Yellow and blue spheres show the DFT-optimized positions of X = Ag by treating the total cluster charge as q = 6 and 8, respectively.

intensity peaks around 381 and 349 nm (Figure S3a and Table S1). The computed spectrum reproduces these three distinct peaks (labeled 1, 2, and 3 in Figure 5a), although the
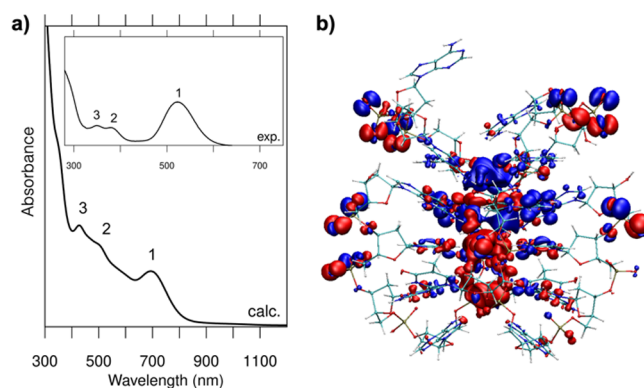

Figure 5. (a) Calculated UV−vis absorption spectrum of A10-$(DNA)_2[Ag_{16}Cl_2]^{8+}$ (atom positions taken from ref 32) as compared to the experimental data (inset). Although red-shifted with respect to the measured spectrum, the calculated spectrum reproduces the features 1−3 seen in experiment. (b) Induced transition density for the calculated peak 1. Blue and red denote oscillation phases ("charge sloshing") creating the transition dipole.

that chloride ions are stable (the Ag−Cl distance decreased by 0.1 Å). In contrast, when X = Ag, we find that Ag atoms are stable on the metal core surface only for q = 6 (yellow) but not for q = 8 (blue).

We calculated the theoretical absorption spectrum by considering the full crystallographic structure for $(DNA)_2[Ag_{16}Cl_2]^{8+}$ and using the linear-response formulation of the time-dependent DFT.[49] All $(DNA)_2[Ag_{16}Cl_2]^{8+}$ variants show a consistent shape of the experimental UV−vis absorption spectra regardless of the specific DNA template sequence, with a strong peak around 523 nm and two lower-

computed transitions are all red-shifted. Detailed analysis of the character of these peaks will be discussed in a forthcoming theoretical paper, but we summarize the main findings here as follows. All three peaks have major contributions from single electron−hole transitions taking place within the silver core, involving the Cl atoms as well, and with increasing contributions from the DNA nucleobases at the silver−DNA interface for peaks 2 and 3. The induced transition density for the computed lowest-energy peak 1 visualizes oscillation of the electron density in the longitudinal direction of the Ag_{16} core (Figure 5b). This finding agrees with the previous prediction
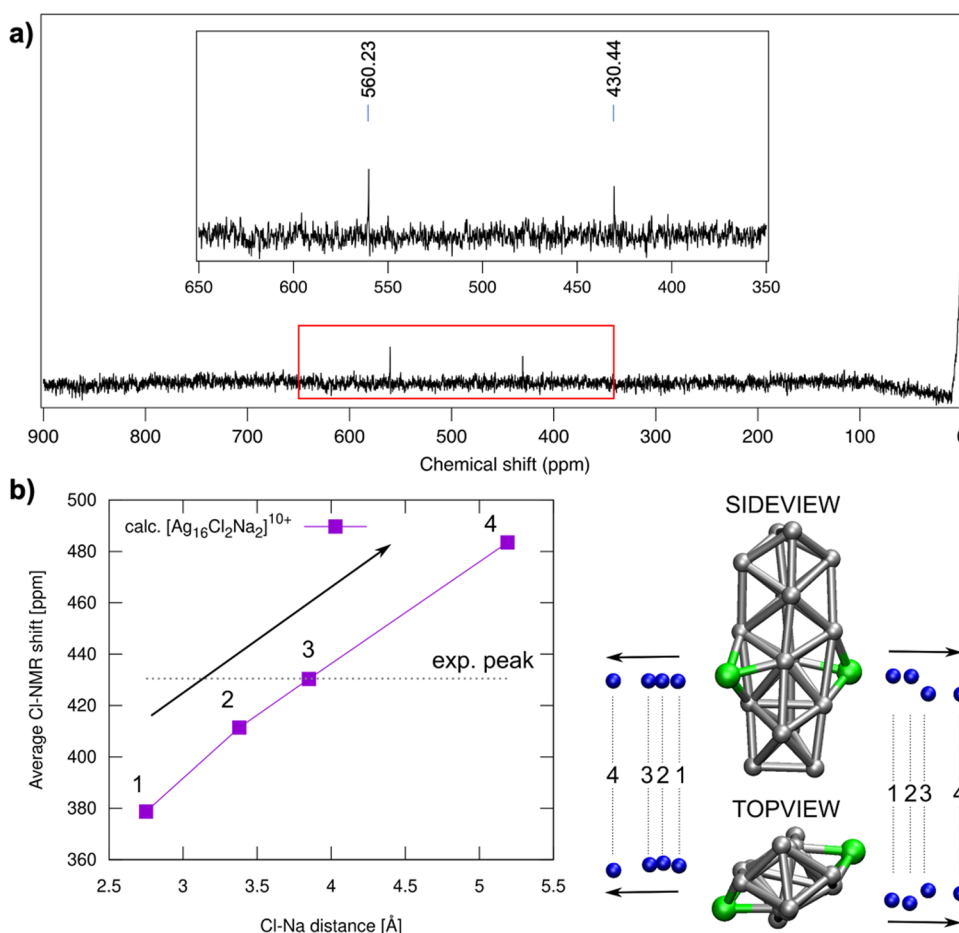
Figure 6. (a) Experimental ^{35}Cl-NMR spectrum of $(DNA)_2[Ag_{16}Cl_2]^{8+}$. The inset shows the area in the red box. The peak at 0 ppm corresponds to free chlorides in solution, in agreement with the reference used (NaCl in D_2O). (b) Proximity effect by Na^+ cations on the ^{35}Cl-NMR shift. The calculations were made on the isolated $[Ag_{16}Cl_2]^{8+}$ cluster (right) where two Na^+ cations (blue spheres) were placed close to Cl atoms (green spheres) in the cluster. The computed ^{35}Cl shifts as a function of the Cl−Na distance are shown on the left, where the horizontal dotted line shows the observed experimental NMR peak at 430.44 ppm.

that longitudinal charge oscillations are responsible for the longest wavelength UV−vis transition of Ag_N-DNAs.[14] Note that the DFT calculations show minor contributions to the lowest-energy peak 1 transition on some phosphate groups, which may be due to neglect of the dielectric environment in the calculations. Future work is needed to explore solvent effects.

^{35}Cl-NMR Measurements and Interpretation by DFT. ^{35}Cl-NMR was performed on $(DNA)_2[Ag_{16}Cl_2]^{8+}$ to further confirm the presence of chloride ligands and interrogate the nature of their interactions with the nanocluster. The ^{35}Cl-NMR spectrum presents two peaks at 560.23 and 430.44 ppm (Figure 6a). The large 130 ppm separation of the peaks suggests that there are two different environments for chloride, in apparent conflict with the fact that the chloride positions (previously assigned as low-occupancy silvers in the crystallographic study) appear approximately equivalent. To decipher this mystery, we resorted to DFT calculations using the deMon2k code[50] (see technical details in the Supporting Information). We computed the reference ^{35}Cl-NMR peak for a model of a solvated Na^+ and Cl^- ion pair in a droplet of 100 water molecules (Figure S21). Using this system as a 0 ppm reference, the two chlorides at the crystallographic sites of the $(DNA)_2[Ag_{16}Cl_2]^{8+}$ nanocluster have calculated NMR chemical shifts of 557.6 and 552.1 ppm, yielding an average value of

554.9 ppm. This average calculated chemical shift corresponds extremely well to one of the experimental peaks at 560.23 ppm (Figure 6a), yielding a firm assignment.

Visual inspection of the $(DNA)_2[Ag_{16}Cl_2]^{8+}$ crystal structure reveals an interesting detail that turns out to be extremely beneficial for a tentative assignment of the second observed ^{35}Cl-NMR peak at 430.44 ppm. As illustrated in Figure S22, Cl sites are accessible from solvent through the DNA. We hypothesize that these "channels" in Figure S22 allow Na^+ ions from the solvent to access the silver−DNA interface, creating a potential proximity effect on the ^{35}Cl-NMR shift. Indeed, by assessing this effect via systematic DFT deMon2k calculations, we find that the shift is quite sensitive to the distance between Na^+ and the chlorides of $[Ag_{16}Cl_2]^{8+}$, and values around 4 Å yield a shift very close to the measured shift (Figure 6b). Thus, we assign the 430.44 ppm peak to this proximity effect. Na^+ ions "trapped" at the silver−DNA interface close to Cl may also account for some of the observed Na^+ adducts in the ESI-MS data (Figure S11). We note that luminescence properties of Ag_N clusters within zeolites can be significantly modulated by counter-balancing ions,[51,52] and future studies could explore whether similar effects exist for Ag_N-DNAs.

Crystal Structure Refinement. The crystal structure of the A10 variant[32] was refined using the program phenix.refine in the Phenix suite[53] by replacing the original Ag atoms of low
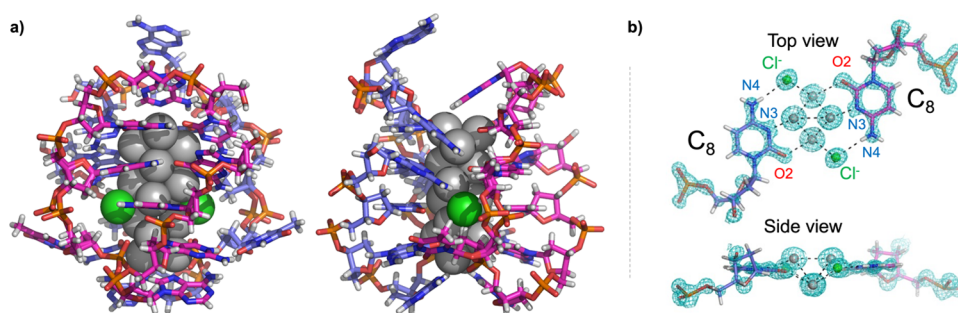
Figure 7. (a) Overall structure of $(DNA)_2[Ag_{16}Cl_2]^{8+}$. (b) $2|F_o| - |F_c|$ map around an Ag-mediated C8–C8 base pair contoured at the 1.5σ level. (Silver: Ag atoms; green: Cl$^-$ ions.) Structural details available at the PDB database using accession code 6M2P.

occupancies (0.33 and 0.34 in ref 32, PDB accession code 6M2P) with Cl$^-$ ions of occupancy 1 (Figure 7). A comparison of the statistics of structure refinement (Table S5) shows that both R-factor and R_{free} do not change before and after the refinement, confirming that the nanocluster core consists of 16 Ag atoms and 2 Cl$^-$ ions. Figure 7b shows the top and side views of the Ag-mediated C_8–C_8 base pair (C_8 refers to the cytosine in position 8 of the DNA template strand). Four Ag atoms and two Cl$^-$ ions are almost on the same plane as the two C_8 bases. Ag atoms constituting the Ag_{16} core coordinate to O2 and N3 of the C_8 bases. The Cl$^-$ ion makes a Cl···H−N hydrogen bond with the amino group at the N4 position of the C_8 base and coordinates with an Ag atom. As can be seen from the top view, the Cl$^-$ ions are arranged against the Ag atom in the same way as the O2 atoms, yielding a coordination structure that appears to be highly symmetric.

Chloride Ligands on Other Ag$_N$-DNAs. Finally, we investigate the possibility that other DNA-stabilized silver nanoclusters possess mixed DNA/chloride ligands. In this study, we observed that compared to most Ag$_N$-DNAs, the fluorescence emission spectrum of unpurified $(DNA)_2[Ag_{16}Cl_2]^{8+}$ is unusually stable in saline media, including 0.9% NaCl and phosphate buffered saline (PBS) (50 mM KH$_2$PO$_4$, 100 mM NaCl) (Figure S23). Therefore, we experimentally screened a set of 372 Ag$_N$-DNAs that were designed by machine learning methods[8] to identify other nanocluster species with spectral stability in 0.9% NaCl and PBS. Several species satisfying these criteria were then synthesized without adding any chloride salts, purified by HPLC, and sized by ESI-MS to identify ligand composition. By this method, we found that 5′-AACCCCACGT-3′ from Mastracco et al.[8] stabilizes a red-emissive product with 500 nm peak absorbance and 650 nm peak emission that can be isolated successfully by HPLC and has composition $(DNA)_2[Ag_{15}Cl]^{8+}$ (Figures S24–S26). These results show that Ag$_N$-DNAs that present chloride ligands without intentional addition of chloride salts may be prevalent in experiments. Moreover, both Ag$_N$-DNAs with chloride ligands have larger Stokes shifts than most previously reported Ag$_N$-DNAs.[36] Previous theoretical studies of the Ag−AgCl interface at the nanocluster scale reported formation of new electronic states at the interface, which may influence optical properties.[54] Future theoretical studies may clarify how ligand chemistry affects the excited-state properties of Ag$_N$-DNAs.

CONCLUSIONS

We show that the well-studied NIR-emissive Ag$_N$-DNAs, with previously reported crystal structures, have the molecular formula $(DNA)_2[Ag_{16}Cl_2]^{8+}$. This is the first report of DNA-stabilized nanoclusters with mixed DNA and chloride ligands. Mass spectral analysis also assigns the 6-electron count of this nanocluster, enabling DFT calculations to solve the electronic structure of Ag$_N$-DNA species for the first time. DFT calculations also interpret the ^{35}Cl-NMR spectrum of this nanocluster species and show the presence of a channel that enables Na$^+$ ions to approach the chloride ligands, producing a distinct NMR signature and possibly facilitating halide ligand exchange. Reanalysis of the X-ray crystal structure is consistent with the assignment of the nanocluster as containing 16 Ag and 2 Cl atoms. The chloride ligands appear to confer additional chemical stability to the NIR-emissive $(DNA)_2[Ag_{16}Cl_2]^{8+}$, and this heightened stability is used to identify one additional Ag$_N$-DNA that possesses mixed DNA/chloride ligands.

Ag$_N$-DNAs have been reported as promising emitters for a range of biomedical applications, from sensing to bioimaging.[2,55,56] To advance such applications, it is critical to achieve Ag$_N$-DNA species that possess chemical stability in the presence of physiologically relevant ∼100 mM concentrations of chloride.[57] Thus, the added stability conferred to Ag$_N$-DNAs with mixed DNA/chloride ligands presents a promising new route to expand these emitters for practical applications in biomedical research. We note that the Ag$_N$-DNAs with a mixed chloride/DNA ligand composition found here were synthesized without intentional addition of chloride. Future studies should determine synthetic strategies to intentionally achieve mixed ligand Ag$_N$-DNAs, which could significantly expand the structure−property relationships and applications of these emitters.

■ EXPERIMENTAL SECTION

Nanocluster Synthesis and Purification. All Ag$_N$-DNAs were synthesized by mixing single-strand DNA oligomers (Integrated DNA Technologies, standard desalting) with AgNO$_3$ in a 10 mM ammonium acetate (NH$_4$OAc) solution, pH 7 without additional chloride salts. After 15 min, a 0.5 molar fraction of NaBH$_4$ to AgNO$_3$ was added to partially reduce the silver cations. Samples were purified 5 days after synthesis using reverse-phase HPLC (see the Supporting Information for additional synthesis details).

Optical Characterization. Absorbance and emission spectra of purified Ag$_N$-DNAs were collected using a thermoelectrically cooled, fiber-coupled spectrometer (Ocean Optics QE65000). Absorbance spectra were collected using a DH-Mini (Ocean Insight) deuterium and tungsten halogen UV−vis−NIR light source. Fluorescence spectra were collected using a UV LED as a light source for universal UV-excitation of the nanoclusters.[58]

Mass Spectrometry. ESI-MS measurements were performed on the same day as optical characterization in a Waters Xevo G2-XS QTof. Samples were directly injected at 0.1 mL·min^{-1} in negative ion mode with a 2 kV capillary voltage, 30 V cone voltage, and no collision energy. Spectra were collected from 1000 to 4000 m/z and

integrated for 1 s. Source and desolvation temperatures were 80 and 150 °C, respectively. Gas flows were 45 L/h for the cone and 450 L/h for the desolvation. All samples were injected with 50 mM NH_4OAc–MeOH (80:20) buffer at pH 7. The instrument was calibrated using a 2 μg/L solution of CsI. Nanocluster size and charge were determined by fitting the predicted isotopic distribution of the Ag_N-DNA using MassLynx software to the experimental spectra.

^{35}Cl NMR. ^{35}Cl-NMR measurements were performed on a 300 MHz Bruker Avance HD III HD Nanobay NMR spectrometer for a sample exchanged into D_2O. External NaCl in D_2O was used as a 0 ppm reference. Detailed methods are provided in the Supporting Information.

DFT Calculations. The ground-state electronic structure of the A10-$(DNA)_2[Ag_{16}Cl_2]^{8+}$ variant species was investigated using the DFT code GPAW (ref 48), and the optical spectrum was calculated using the linear-response time-dependent DFT extension in the code (ref 49). The chemical shifts of Cl atoms were calculated for the $[Ag_{16}Cl_{12}]^{8+}$ inorganic core of the A10-species using the DFT code deMon2k (ref 50).

ASSOCIATED CONTENT

ⓈⒾ Supporting Information

The Supporting Information is available free of charge at https://pubs.acs.org/doi/10.1021/jacs.3c01366.

> Materials and experimental methods, computational methods, HPLC chromatograms, optical spectra of purified Ag_N-DNAs, mass spectra and calculated mass distributions, DFT calculations for interpretations of ^{35}Cl-NMR measurements, and crystallographic reanalysis tables (PDF)

AUTHOR INFORMATION

Corresponding Author

Stacy M. Copp − Department of Materials Science and Engineering, Department of Physics and Astronomy, and Department of Chemical and Biomolecular Engineering, University of California, Irvine, California 92697, United States; ⓞ orcid.org/0000-0002-1788-1778; Email: stacy.copp@uci.edu

Authors

Anna Gonzàlez-Rosell − Department of Materials Science and Engineering, University of California, Irvine, California 92697, United States; ⓞ orcid.org/0000-0001-6899-8901

Sami Malola − Departments of Chemistry and Physics, Nanoscience Center, University of Jyväskylä, Jyväskylä 40014, Finland

Rweetuparna Guha − Department of Materials Science and Engineering, University of California, Irvine, California 92697, United States; ⓞ orcid.org/0000-0001-7879-2165

Nery R. Arevalos − Department of Materials Science and Engineering, University of California, Irvine, California 92697, United States; ⓞ orcid.org/0000-0001-8186-1467

María Francisca Matus − Departments of Chemistry and Physics, Nanoscience Center, University of Jyväskylä, Jyväskylä 40014, Finland; ⓞ orcid.org/0000-0002-4816-531X

Meghen E. Goulet − Department of Chemistry, University of California, Irvine, California 92697, United States

Esa Haapaniemi − Department of Chemistry, University of Jyväskylä, Jyväskylä 40014, Finland

Benjamin B. Katz − Department of Chemistry, University of California, Irvine, California 92697, United States

Tom Vosch − Nanoscience Center and Department of Chemistry, University of Copenhagen, Copenhagen 2100, Denmark; ⓞ orcid.org/0000-0001-5435-2181

Jiro Kondo − Department of Materials and Life Sciences, Faculty of Science and Technology, Sophia University, Tokyo 102-8554, Japan; ⓞ orcid.org/0000-0002-5682-3685

Hannu Häkkinen − Departments of Chemistry and Physics, Nanoscience Center, University of Jyväskylä, Jyväskylä 40014, Finland; ⓞ orcid.org/0000-0002-8558-5436

Complete contact information is available at:
https://pubs.acs.org/10.1021/jacs.3c01366

Notes

The authors declare no competing financial interest.

ACKNOWLEDGMENTS

REFERENCES

(1) Petty, J. T.; Zheng, J.; Hud, N. V.; Dickson, R. M. DNA-Templated Ag Nanocluster Formation. *J. Am. Chem. Soc.* **2004**, *126*, 5207−5212.

(2) Chen, Y.; Phipps, M. L.; Werner, J. H.; Chakraborty, S.; Martinez, J. S. DNA Templated Metal Nanoclusters: From Emergent Properties to Unique Applications. *Acc. Chem. Res.* **2018**, *51*, 2756−2763.

(3) Gonzàlez-Rosell, A.; Cerretani, C.; Mastracco, P.; Vosch, T.; Copp, S. M. Structure and Luminescence of DNA-Templated Silver Clusters. *Nanoscale Adv.* **2021**, *3*, 1230−1260.

(4) Xu, C.; Pu, F.; Ren, J.; Qu, X. A DNA/Metal Cluster-Based Nano-Lantern as an Intelligent Theranostic Device. *Chem. Commun.* **2020**, *56*, 5295−5298.

(5) Kim, S.; Lee, E. S.; Cha, B. S.; Park, K. S. High Fructose Concentration Increases the Fluorescence Stability of DNA-Templated Copper Nanoclusters by Several Thousand Times. *Nano Lett.* **2022**, *22*, 6121−6127.

(6) Ran, X.; Wang, Z.; Pu, F.; Ju, E.; Ren, J.; Qu, X. Nucleic Acid-Driven Aggregation-Induced Emission of Au Nanoclusters for Visualizing Telomerase Activity in Living Cells and in Vivo. *Mater. Horiz.* **2021**, *8*, 1769−1775.

(7) Huard, D. J. E.; Demissie, A.; Kim, D.; Lewis, D.; Dickson, R. M.; Petty, J. T.; Lieberman, R. L. Atomic Structure of a Fluorescent Ag8 Cluster Templated by a Multistranded DNA Scaffold. *J. Am. Chem. Soc.* **2019**, *141*, 11465−11470.

(8) Mastracco, P.; Gonzàlez-Rosell, A.; Evans, J.; Bogdanov, P.; Copp, S. M. Chemistry-Informed Machine Learning Enables Discovery of DNA-Stabilized Silver Nanoclusters with Near-Infrared Fluorescence. *ACS Nano* **2022**, *16*, 16322−16331.

(9) Vosch, T.; Antoku, Y.; Hsiang, J.-C.; Richards, C. I.; Gonzalez, J. I.; Dickson, R. M. Strongly Emissive Individual DNA-Encapsulated Ag Nanoclusters as Single-Molecule Fluorophores. *Proc. Natl. Acad. Sci. U. S. A.* **2007**, *104*, 12616−12621.

(10) Petty, J. T.; Carnahan, S.; Kim, D.; Lewis, D. Long-Lived Ag106+ Luminescence and a Split DNA Scaffold. *J. Chem. Phys.* **2021**, *154*, 244302.

(11) Rück, V.; Cerretani, C.; Neacşu, V. A.; Liisberg, M. B.; Vosch, T. Observation of Microsecond Luminescence While Studying Two DNA-Stabilized Silver Nanoclusters Emitting in the 800−900 Nm Range. *Phys. Chem. Chem. Phys.* **2021**, *23*, 13483−13489.

(12) Gonzàlez-Rosell, A.; Guha, R.; Cerretani, C.; Rück, V.; Liisberg, M. B.; Katz, B. B.; Vosch, T.; Copp, S. M. DNA Stabilizes Eight-Electron Superatom Silver Nanoclusters with Broadband Down-conversion and Microsecond-Lived Luminescence. *J. Phys. Chem. Lett.* **2022**, 8305−8311.

(13) Schultz, D.; Gardner, K.; Oemrawsingh, S. S. R.; Markeševič, N.; Olsson, K.; Debord, M.; Bouwmeester, D.; Gwinn, E. Evidence for Rod-Shaped DNA-Stabilized Silver Nanocluster Emitters. *Adv. Mater.* **2013**, *25*, 2797−2803.

(14) Copp, S. M.; Schultz, D.; Swasey, S. M.; Faris, A.; Gwinn, E. G. Cluster Plasmonics: Dielectric and Shape Effects on DNA-Stabilized Silver Clusters. *Nano Lett.* **2016**, *16*, 3594−3599.

(15) Neacşu, V. A.; Cerretani, C.; Liisberg, M.; Swasey, S. M.; Gwinn, E. G.; Copp, S. M.; Vosch, T. Unusually Large Fluorescence Quantum Yield for a Near-Infrared Emitting DNA-Stabilized Silver Nanocluster. *Chem. Commun.* **2020**, *56*, 6384.

(16) Gwinn, E. G.; O'Neill, P.; Guerrero, A. J.; Bouwmeester, D.; Fygenson, D. K. Sequence-Dependent Fluorescence of DNA-Hosted Silver Nanoclusters. *Adv. Mater.* **2008**, *20*, 279−283.

(17) Schultz, D.; Gwinn, E. G. Silver Atom and Strand Numbers in Fluorescent and Dark Ag:DNAs. *Chem. Commun.* **2012**, *48*, 5748−5750.

(18) Fleischer, B. C.; Petty, J. T.; Hsiang, J.-C.; Dickson, R. M. Optically Activated Delayed Fluorescence. *J. Phys. Chem. Lett.* **2017**, *8*, 3536−3543.

(19) Krause, S.; Cerretani, C.; Vosch, T. Disentangling Optically Activated Delayed Fluorescence and Upconversion Fluorescence in DNA Stabilized Silver Nanoclusters. *Chem. Sci.* **2019**, *10*, 5326−5331.

(20) Thyrhaug, E.; Bogh, S. A.; Carro-Temboury, M. R.; Madsen, C. S.; Vosch, T.; Zigmantas, D. Ultrafast Coherence Transfer in DNA-Templated Silver Nanoclusters. *Nat. Commun.* **2017**, *8*, 15577.

(21) Swasey, S. M.; Copp, S. M.; Nicholson, H. C.; Gorovits, A.; Bogdanov, P.; Gwinn, E. G. High Throughput near Infrared Screening Discovers DNA-Templated Silver Clusters with Peak Fluorescence beyond 950 Nm. *Nanoscale* **2018**, *10*, 19701−19705.

(22) Moomtaheen, F.; Killeen, M.; Oswald, J.; Gonzàlez-Rosell, A.; Mastracco, P.; Gorovits, A.; Copp, S. M.; Bogdanov, P. DNA-Stabilized Silver Nanocluster Design via Regularized Variational Autoencoders. In *Proceedings of the 28th ACM SIGKDD International Conference on Knowledge Discovery & Data Mining*; 2022.

(23) Bogh, S. A.; Carro-Temboury, M. R.; Cerretani, C.; Swasey, S. M.; Copp, S. M.; Gwinn, E. G.; Vosch, T. Unusually Large Stokes Shift for a Near-Infrared Emitting DNA-Stabilized Silver Nanocluster. *Methods Appl. Fluoresc.* **2018**, *6*, No. 024004.

(24) Krause, S.; Carro-Temboury, M. R.; Cerretani, C.; Vosch, T. Probing Heterogeneity of NIR Induced Secondary Fluorescence from DNA-Stabilized Silver Nanoclusters at the Single Molecule Level. *Phys. Chem. Chem. Phys.* **2018**, *20*, 16316−16319.

(25) Liisberg, M. B.; Kardar, Z. S.; Copp, S. M.; Cerretani, C.; Vosch, T. Single-Molecule Detection of DNA-Stabilized Silver Nanoclusters Emitting at the NIR I/II Border. *J. Phys. Chem. Lett.* **2021**, *12*, 1150−1154.

(26) Liisberg, M. B.; Krause, S.; Cerretani, C.; Vosch, T. Probing Emission of a DNA-Stabilized Silver Nanocluster from the Sub-Nanosecond to Millisecond Timescale in a Single Measurement. *Chem. Sci.* **2022**, *13*, 5582−5587.

(27) Jin, R.; Zeng, C.; Zhou, M.; Chen, Y. Atomically Precise Colloidal Metal Nanoclusters and Nanoparticles: Fundamentals and Opportunities. *Chem. Rev.* **2016**, *116*, 10346−10413.

(28) Koszinowski, K.; Ballweg, K. A Highly Charged Ag₆⁴⁺ Core in a DNA-Encapsulated Silver Nanocluster. *Chem. — Eur. J.* **2010**, *16*, 3285−3290.

(29) Copp, S. M.; Schultz, D.; Swasey, S.; Pavlovich, J.; Debord, M.; Chiu, A.; Olsson, K.; Gwinn, E. Magic Numbers in DNA-Stabilized Fluorescent Silver Clusters Lead to Magic Colors. *J. Phys. Chem. Lett.* **2014**, *5*, 959−963.

(30) Walter, M.; Akola, J.; Lopez-Acevedo, O.; Jadzinsky, P. D.; Calero, G.; Ackerson, C. J.; Whetten, R. L.; Grönbeck, H.; Häkkinen,

H. A Unified View of Ligand-Protected Gold Clusters as Superatom Complexes. *Proc. Natl. Acad. Sci. U. S. A.* **2008**, *105*, 9157−9162.

(31) Cerretani, C.; Kanazawa, H.; Vosch, T.; Kondo, J. Crystal Structure of a NIR-Emitting DNA-Stabilized Ag₁₆ Nanocluster. *Angew. Chem., Int. Ed.* **2019**, *58*, 17153−17157.

(32) Cerretani, C.; Kondo, J.; Vosch, T. Removal of the A10 Adenosine in a DNA-Stabilized Ag16 Nanocluster. *RSC Adv.* **2020**, *10*, 23854−23860.

(33) Cerretani, C.; Kondo, J.; Vosch, T. Mutation of Position 5 as a Crystal Engineering Tool for a NIR-Emitting DNA-Stabilized Ag16nanocluster. *CrystEngComm* **2020**, *22*, 8136−8141.

(34) Cerretani, C.; Liisberg, M. B.; Rück, V.; Kondo, J.; Vosch, T. The Effect of Inosine on the Spectroscopic Properties and Crystal Structure of a NIR-Emitting DNA-Stabilized Silver Nanocluster. *Nanoscale Adv.* **2022**, *4*, 3212−3217.

(35) Largy, E.; König, A.; Ghosh, A.; Ghosh, D.; Benabou, S.; Rosu, F.; Gabelica, V. Mass Spectrometry of Nucleic Acid Noncovalent Complexes. *Chem. Rev.* **2022**, *122*, 7720−7839.

(36) Copp, S. M.; Gonzàlez-Rosell, A. Large-Scale Investigation of the Effects of Nucleobase Sequence on Fluorescence Excitation and Stokes Shifts of DNA-Stabilized Silver Clusters. *Nanoscale* **2021**, *13*, 4602−4613.

(37) Zeng, J. L.; Guan, Z. J.; Du, Y.; Nan, Z. A.; Lin, Y. M.; Wang, Q. M. Chloride-Promoted Formation of a Bimetallic Nanocluster Au80Ag30 and the Total Structure Determination. *J. Am. Chem. Soc.* **2016**, *138*, 7848−7851.

(38) Hu, F.; Li, J.; Guan, Z.; Yuan, S.; Wang, Q. Formation of an Alkynyl-Protected Ag₁₁₂ Silver Nanocluster as Promoted by Chloride Released In Situ from CH₂Cl₂. *Angew. Chem., Int. Ed.* **2020**, *59*, 5312−5315.

(39) Li, J. J.; Guan, Z. J.; Yuan, S. F.; Hu, F.; Wang, Q. M. Enriching Structural Diversity of Alkynyl-Protected Gold Nanoclusters with Chlorides. *Angew. Chem., Int. Ed.* **2021**, *60*, 6699−6703.

(40) Liu, J.-Y.; Alkan, F.; Wang, Z.; Zhang, Z.-Y.; Kurmoo, M.; Yan, Z.; Zhao, Q.-Q.; Aikens, C. M.; Tung, C.-H.; Sun, D. Different Silver Nanoparticles in One Crystal: Ag₂₁₀(ⁱPrPhS)₇₁(Ph₃P)₅Cl and Ag₂₁₁(ⁱPrPhS)₇₁(Ph₃P)₆Cl. *Angew. Chem., Int. Ed.* **2019**, *58*, 195−199.

(41) Touchton, A. J.; Wu, G.; Hayton, T. W. [Ni8(CNtBu)12][Cl]: A Nickel Isocyanide Nanocluster with a Folded Nanosheet Structure. *J. Chem. Phys.* **2021**, *154*, 211102.

(42) Kulkarni, V. K.; Khiarak, B. N.; Takano, S.; Malola, S.; Albright, E. L.; Levchenko, T. I.; Aloisio, M. D.; Dinh, C. T.; Tsukuda, T.; Häkkinen, H.; Crudden, C. M. N-Heterocyclic Carbene-Stabilized Hydrido Au24Nanoclusters: Synthesis, Structure, and Electrocatalytic Reduction of CO2. *J. Am. Chem. Soc.* **2022**, *144*, 9000−9006.

(43) Touchton, A. J.; Wu, G.; Hayton, T. W. Revisited: Isolation and Characterization of [Ni23Se12Cl3(PEt3)10]. *Inorg. Chem.* **2021**, *60*, 17586−17592.

(44) Lummis, P. A.; Osten, K. M.; Levchenko, T. I.; Sabooni Asre Hazer, M.; Malola, S.; Owens-Baird, B.; Veinot, A. J.; Albright, E. L.; Schatte, G.; Takano, S.; Kovnir, K.; Stamplecoskie, K. G.; Tsukuda, T.; Häkkinen, H.; Nambo, M.; Crudden, C. M. NHC-Stabilized Au10 Nanoclusters and Their Conversion to Au25 Nanoclusters. *J. Am. Chem. Soc.* **2022**, *2*, 875−885.

(45) Tlahuice-Flores, A.; Black, D. M.; Bach, S. B. H.; Jose-Yacamán, M.; Whetten, R. L. Structure & Bonding of the Gold-Subhalide Cluster I-Au₁₄₄Cl₆₀[Z]. *Phys. Chem. Chem. Phys.* **2013**, *15*, 19191−19195.

(46) Cirri, A.; Hernández, H. M.; Johnson, C. J. Hydride, Chloride, and Bromide Show Similar Electronic Effects in the Au9(PPh3)83+ Nanocluster. *Chem. Commun.* **2020**, *56*, 1283−1285.

(47) Man, R. W. Y.; Yi, H.; Malola, S.; Takano, S.; Tsukuda, T.; Häkkinen, H.; Nambo, M.; Crudden, C. M. Synthesis and Characterization of Enantiopure Chiral Bis NHC-Stabilized Edge-Shared Au10Nanocluster with Unique Prolate Shape. *J. Am. Chem. Soc.* **2022**, *144*, 2056−2061.

(48) Enkovaara, J.; Rostgaard, C.; Mortensen, J. J.; Chen, J.; Dułak, M.; Ferrighi, L.; Gavnholt, J.; Glinsvad, C.; Haikola, V.; Hansen, H.

A.; Kristoffersen, H. H.; Kuisma, M.; Larsen, A. H.; Lehtovaara, L.; Ljungberg, M.; Lopez-Acevedo, O.; Moses, P. G.; Ojanen, J.; Olsen, T.; Petzold, V.; Romero, N. A.; Stausholm-Møller, J.; Strange, M.; Tritsaris, G. A.; Vanin, M.; Walter, M.; Hammer, B.; Häkkinen, H.; Madsen, G. K. H.; Nieminen, R. M.; Nørskov, J. K.; Puska, M.; Rantala, T. T.; Schiøtz, J.; Thygesen, K. S.; Jacobsen, K. W. Electronic Structure Calculations with GPAW: A Real-Space Implementation of the Projector Augmented-Wave Method. *J. Phys.: Condens. Matter* **2010**, *25*, No. 253202.

(49) Walter, M.; Häkkinen, H.; Lehtovaara, L.; Puska, M.; Enkovaara, J.; Rostgaard, C.; Mortensen, J. J. Time-Dependent Density-Functional Theory in the Projector Augmented-Wave Method. *J. Chem. Phys.* **2008**, *128*, 244101.

(50) Köster, A. M.; Geudtner, G.; Alvarez-Ibarra, A.; Calaminici, P.; Casida, M. E.; Carmona-Espindola, J.; Dominguez, V. D.; Flores-Moreno, R.; Gamboa, G. U.; Goursot, A.; Heine, T.; Ipatov, A.; de la Lande, A.; Janetzko, F.; del Campo, J. M.; Mejia-Rodriguez, D.; Reveles, J. U.; Vasquez-Perez, J.; Vela, A.; Zuniga-Gutierrez, B.; Salahub, D. R. *DeMon2k, Version 6*; The deMon Developers: Cinvestav, Mexico City, 2018.

(51) De Cremer, G.; Coutiño-Gonzalez, E.; Roeffaers, M. B. J.; Moens, B.; Ollevier, J.; Van Der Auweraer, M.; Schoonheydt, R.; Jacobs, P. A.; De Schryver, F. C.; Hofkens, J.; De Vos, D. E.; Sels, B. F.; Vosch, T. Characterization of Fluorescence in Heat-Treated Silver-Exchanged Zeolites. *J. Am. Chem. Soc.* **2009**, *131*, 3049−3056.

(52) Coutino-Gonzalez, E.; Baekelant, W.; Grandjean, D.; Roeffaers, M. B. J.; Fron, E.; Aghakhani, M. S.; Bovet, N.; Van Der Auweraer, M.; Lievens, P.; Vosch, T.; Sels, B.; Hofkens, J. Thermally Activated LTA(Li)−Ag Zeolites with Water-Responsive Photoluminescence Properties. *J. Mater. Chem. C* **2015**, *3*, 11857−11867.

(53) Afonine, P. V.; Grosse-Kunstleve, R. W.; Echols, N.; Headd, J. J.; Moriarty, N. W.; Mustyakimov, M.; Terwilliger, T. C.; Urzhumtsev, A.; Zwart, P. H.; Adams, P. D. Towards Automated Crystallographic Structure Refinement with Phenix.Refine. *Acta Crystallogr. Sect., D: Biol. Crystallogr.* **2012**, *68*, 352−367.

(54) Glaus, S.; Calzaferri, G.; Hoffmann, R. Electronic Properties of the Silver-Silver Chloride Cluster Interface. *Chem. − Eur. J.* **2002**, *8*, 1785−1794.

(55) Hong, S.; Kuo, Y.-A.; Nguyen, T. D.; Chen, Y.-I.; Liu, Y.-L.; Shankar, P. B.; Yeh, H.-C. Array-Based Differential Sensing of Cancer Cells Using DNA-Templated Silver Nanoclusters. In *Nanoscale Imaging, Sensing, and Actuation for Biomedical Applications XVII*; Fixler, D.; Wachsmann-Hogiu, S.; Goldys, E. M., Eds.; SPIE - The International Society for Optical Engineering; 2020; vol *11254*, p 34.

(56) Lyu, D.; Li, J.; Wang, X.; Guo, W.; Wang, E. Cationic-Polyelectrolyte-Modified Fluorescent DNA−Silver Nanoclusters with Enhanced Emission and Higher Stability for Rapid Bioimaging. *Anal. Chem.* **2019**, *91*, 2050−2057.

(57) Dick, D. A. The Distribution of Sodium, Potassium and Chloride in the Nucleus and Cytoplasm of Bufo Bufo Oocytes Measured by Electron Microprobe Analysis. *J. Physiol.* **1978**, *284*, 37−53.

(58) O'Neill, P. R.; Gwinn, E. G.; Fygenson, D. K. UV Excitation of DNA Stabilized Ag Cluster Fluorescence via the DNA Bases. *J. Phys. Chem. C* **2011**, *115*, 24061−24066.